

**Direct growth of nickel disilicide nanocrystals in silicon dioxide films**

Jong-Hwan Yoon, Gyu-Hyun Lee, and Robert G. Elliman

Citation: *Journal of Applied Physics* **99**, 116106 (2006); doi: 10.1063/1.2202740

View online: <http://dx.doi.org/10.1063/1.2202740>

View Table of Contents: <http://scitation.aip.org/content/aip/journal/jap/99/11?ver=pdfcov>

Published by the [AIP Publishing](#)

---



## Re-register for Table of Content Alerts

Create a profile.



Sign up today!



## Direct growth of nickel disilicide nanocrystals in silicon dioxide films

Jong-Hwan Yoon<sup>a)</sup> and Gyu-Hyun Lee

*Department of Physics, Kangwon National University, Chuncheon, Kangwon-do 200-701, Korea*

Robert G. Elliman

*Department of Electronic Materials Engineering, Research School of Physical Sciences and Engineering, The Australian National University, Canberra, Australian Capital Territory 0200, Australia*

(Received 3 March 2006; accepted 31 March 2006; published online 13 June 2006)

Nickel disilicide ( $\text{NiSi}_2$ ) nanocrystals (NCs) have been grown in silicon-rich oxide ( $\text{SiO}_x$ ) films ion implanted with nickel by annealing at  $1100^\circ\text{C}$ . It was found that  $\text{NiSi}_2$  NCs grew into well-defined single crystalline structures embedded in a  $\text{SiO}_x$  matrix and were approximately spherical in shape. The size of NCs can be influenced by limiting either the Ni or excess Si concentration. It was found that the resulting NCs could be produced with diameters in the range from 5 to 40 nm in the  $\text{SiO}_x$  layers with excess Si concentrations of 4–8 at. % implanted with Ni concentrations of 0.1–10 at. %. © 2006 American Institute of Physics. [DOI: 10.1063/1.2202740]

Semiconductor devices continue to shrink and many rely on quantum phenomena associated with electrons and atoms. Such devices require special fabrication technologies to reach their full potential and these often require different approaches to those employed in present microelectronics. For example, a single-electron quantum dot (QD) transistor, a device called a single-electron tunneling (SET) transistor, has attracted much attention.<sup>1–5</sup> This device is based on an intrinsically quantum phenomenon: the tunnel effect. It exploits the quantized transfer of electrons through the insulating barrier between quantum dot and source/drain,<sup>6</sup> as proposed in principle by Averin and Likharev.<sup>7</sup> The sufficient conditions to operate a SET transistor are that the QD electron charging energy ( $e^2/2C$ , where  $e$  is the charge of an electron and  $C$  is the capacitance of QD) is higher than thermal fluctuation energy ( $k_B T$ , where  $k_B$  is Boltzmann's constant), and that the resistance of the insulator between QD and source/drain is larger than the quantum resistance ( $h/e^2$ , where  $h$  is Planck's constants). To make a SET QD transistor operate well at room temperature, the size of the quantum dot has to be smaller than 15 nm and embedded in a highly insulating material such as silicon dioxide. Here we report the direct growth of crystalline nickel disilicide ( $\text{NiSi}_2$ ) nanocrystals (NCs) in silicon-rich silicon oxide ( $\text{SiO}_x$ ) layers. We show that the  $\text{NiSi}_2$  NCs grow into well-defined single crystalline structures embedded in a  $\text{SiO}_x$  matrix, and that their size can be directly influenced by adjusting the concentrations of either silicon or nickel in a  $\text{SiO}_x$  layer.

Nickel disilicide NCs were formed by thermally annealing Ni implanted silicon-rich silicon oxide ( $\text{SiO}_x$ ) films. Thin ( $\sim 200$  nm)  $\text{SiO}_x$  films of various Si concentrations were deposited on (100) Czochralski silicon wafers at a substrate temperature of  $300^\circ\text{C}$  by plasma-enhanced chemical vapor deposition (PECVD) using a fixed flow rate of  $\text{SiH}_4$  [160 SCCM (SCCM denotes cubic centimeter per minute at STP)] and a variable flow rate of  $\text{NO}_2$  (75 SCCM for  $x=1.70$ , 50 SCCM for  $x=1.56$ , and 35 SCCM for

$x=1.44$ ). The films were subsequently implanted with 130 keV  $\text{Ni}^+$  ions, which resulted in a Ni concentration profile centered in the layer, with a peak ion concentration located at a depth of around 100 nm. The implant fluences were  $6.0 \times 10^{14}$ ,  $6.0 \times 10^{15}$ , and  $6.0 \times 10^{16}$   $\text{cm}^{-2}$ , which nominally correspond to 0.1, 1.0, and 10.0 at. % Ni concentrations, respectively. The Ni concentration profile was confirmed by Rutherford backscattering spectroscopy (RBS) using 2.0 MeV He ions. Nucleation and growth of Ni disilicide NCs were achieved by annealing the Ni implanted  $\text{SiO}_x$  samples at  $1100^\circ\text{C}$  in a quartz-tube furnace using high purity nitrogen gas (99.999%) as an ambient. The microscopic structure of annealed  $\text{SiO}_x$  layers and the size and crystallinity of NCs were studied by transmission electron microscopy (TEM) using a JEOL JEM 2010 instrument operating at 200 kV. The chemical composition of NCs was analyzed by energy dispersive x-ray spectroscopy (EDS) using an energy dispersive spectrometer attached to the TEM instrument. For the EDS analysis, the electron beam was focused to a spot as small as 1.5 nm in size.

Figures 1(a) and 1(b) show cross-sectional transmission electron micrographs (XTEM) of  $\text{SiO}_x$  films ( $x=1.56$ ) without and with 10 at. % Ni concentration, respectively, after annealing at  $1100^\circ\text{C}$  for 4 h. It is seen that the Ni implanted  $\text{SiO}_x$  layer contains a large number of NCs, while the unimplanted layer does not. The average size of the crystallites is larger at the middle of layer where the implanted Ni concentration reaches a maximum. This suggests that the formation of the NCs is related to the local concentration of Ni.

Figure 2 shows a high-magnification XTEM micrograph and associated electron diffraction pattern (inset) obtained from the  $\text{SiO}_x$  layer shown in Fig. 1(b). The XTEM image shows the presence of NCs with well-defined boundaries and approximately spherical shape within the  $\text{SiO}_x$  matrix. The detailed microstructure of the NC marked reveals a regular lattice structure consistent with it being a single crystal phase. This is confirmed by the electron diffraction pattern shown in the inset, which shows diffuse rings consistent with scattering from the amorphous  $\text{SiO}_x$  matrix and discontinuous rings made up of individual diffraction spots, consistent

<sup>a)</sup>Electronic mail: jhyoon@kangwon.ac.kr

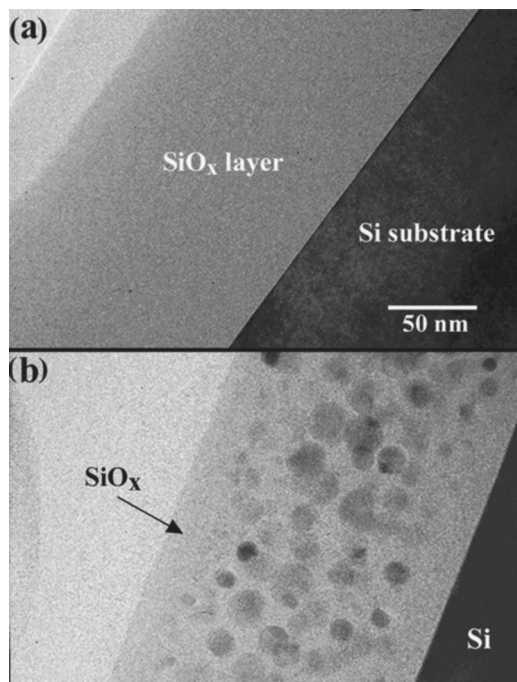


FIG. 1. Cross-sectional transmission electron microscope images of  $\text{SiO}_x$  layers ( $x=1.56$ ) (a) without and (b) with 10 at. % Ni concentration. Note that dark dots, whose size is larger at the middle of layer where the implanted Ni concentration reaches a maximum, are evident in (b) and not in (a).

with diffraction from a low concentration of randomly oriented crystallites.

The  $\text{SiO}_x$  film used in Figs. 1(b) and 2 contains excess Si atoms ( $x=1.56$ ) in addition to the implanted Ni. Annealing such silicon-rich silicon oxide films above 1000 °C generally produces Si nanocrystals<sup>8–10</sup>. However, it is well known that Ni readily reacts with Si to form various Ni silicide phases, the exact phase depending on the ratio of Ni to Si and the annealing temperature.<sup>11–15</sup> The NCs observed in the present samples are therefore likely to be either silicon or Ni silicide crystallites. Using the relation,  $r_1/r_2=d_2/d_1=\sqrt{h_1^2+k_1^2+l_1^2}/\sqrt{h_2^2+k_2^2+l_2^2}$ , where  $r_1$  and  $r_2$  are radii of two rings and  $d_1$  and  $d_2$  are the interplanar spacings of  $(h_1k_1l_1)$  and  $(h_2k_2l_2)$  planes corresponding to rings 1 and 2, respectively, we indexed the diffraction pattern shown in the inset in Fig. 2. This showed that the rings are consistent with the  $\{111\}$ ,  $\{200\}$ ,  $\{220\}$ , and  $\{311\}$  planes of  $\text{NiSi}_2$ .

Exact phase identification is, however, difficult from the electron diffraction patterns alone due to the small volume fraction of crystallites and the similarity between the lattice parameters of Si and various silicide phases (lattice constants both about 0.35 nm)<sup>16</sup>. To assist in this regard energy dispersive EDS was performed on individual NCs. Figure 3 presents representative EDS spectra obtained from outside [Fig. 3(a)] and inside [Fig. 3(b)] a NC. The spectrum presented in Fig. 3(b) was obtained from a NC showing the highest Ni concentration within the field of view. Little, or no Ni is observed in the region between NCs. These qualitative EDS data demonstrate that NCs contain Si and Ni, supporting the premise that they are silicide crystallites. It should be noted, however, that EDS analysis on a range of NCs showed varia-

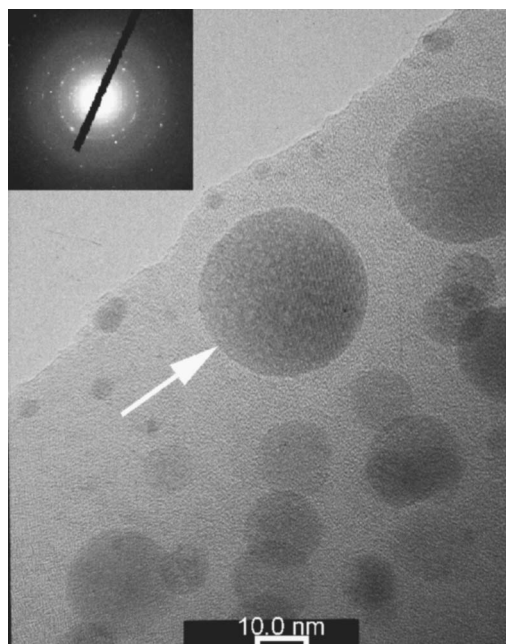


FIG. 2. High-resolution transmission electron micrograph of a sample cross section and associated electron diffraction pattern (inset) taken from a  $\text{SiO}_x$  layer ( $x=1.56$ ) with 10 at. % Ni concentration [the same sample as shown in Fig. 1(b)]. The image shows that the dots are approximately spherical in shape with well-defined boundaries, while the diffraction pattern shows rings composed of bright spots, consistent with a low density of crystallites.

tions in the Ni:Si ratio, ranging from 1:9 up to about 1:2. At least part of this variation arises from the fact that the analysis volume includes regions outside the NC, despite the small lateral size (1.5 nm) of the electron beam.

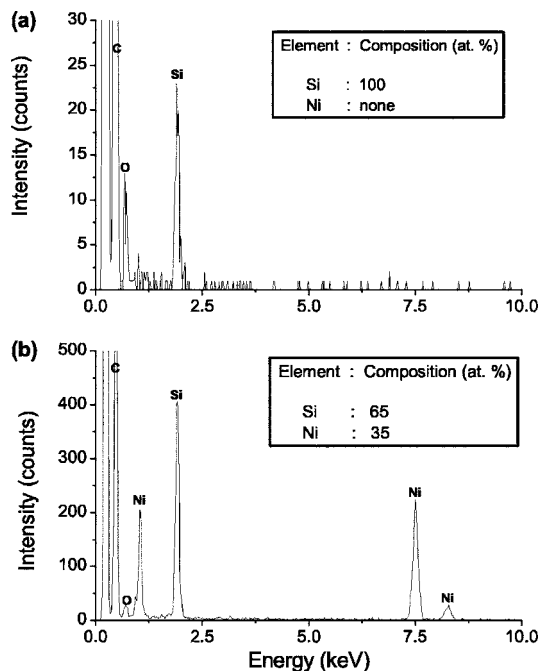


FIG. 3. Representative energy dispersive x-ray (EDS) spectra obtained from a  $\text{SiO}_x$  layer ( $x=1.56$ ) with 10 at. % Ni concentration [the same sample as shown in Figs. 1(b) and 2]. (a) Representative EDS spectrum taken between nanocrystals. (b) Representative EDS spectrum obtained from a dot showing the highest Ni concentration. Note that no significant Ni signal is observed outside of the dots.

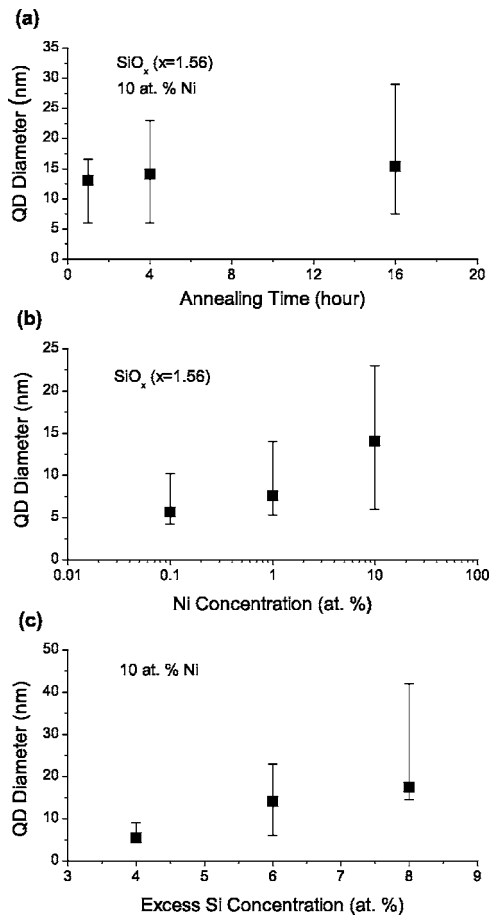


FIG. 4. Nanocrystal (NC) diameters plotted as a function of annealing time, Ni, and Si concentration. (a) Plot of NC diameters obtained from a  $\text{SiO}_x$  layer ( $x=1.56$ ) with a 10 at. % Ni concentration as a function of annealing time. (b) Plot of NC diameters obtained from  $\text{SiO}_x$  layers ( $x=1.56$ ) after annealing at 1100 °C for 4 h as a function of Ni concentration. (c) Plot of NC diameters obtained from  $\text{SiO}_x$  layers with various excess Si concentration and a fixed Ni concentration (10 at. %) after annealing at 1100 °C for 4 h. The filled squares represent the average diameter of NCs, and the bars represent the distribution (minimum-maximum) of NC diameters.

There are many stable Ni silicide phases, depending on the annealing temperature;<sup>17</sup> typically  $\text{Ni}_2\text{Si}$ ,  $\text{NiSi}$ , and  $\text{NiSi}_2$  form for annealing temperatures below 350, 350–750 °C, and above 750 °C, respectively. The NCs presented in the previous figures were formed by annealing at a temperature of 1100 °C, where the stable phase is expected to be nickel disilicide ( $\text{NiSi}_2$ ). In addition, the EDS data show the presence of NCs with Ni concentrations of about 33 at. %, although it varied from NC to NC, similar to that expected in the  $\text{NiSi}_2$  single crystal structure. These data provide strong support for the existence of  $\text{NiSi}_2$  NCs.

Finally, nucleation and growth of  $\text{NiSi}_2$  NCs in the Ni implanted  $\text{SiO}_x$  layers are considered. The annealing-time dependence of NC size, which was obtained from a  $\text{SiO}_x$  layer with  $x=1.56$  (i.e., approximately 6 at. % excess Si) and 10 at. % Ni, as annealed at 1100 °C, is shown in Fig. 4(a). The Ni concentration dependence of NC size obtained from  $\text{SiO}_x$  layers with a fixed concentration of Si ( $x=1.56$ ) and the Si concentration dependence of NC size obtained from  $\text{SiO}_x$  layers with a fixed concentration of Ni (10 at. %), which were annealed at 1100 °C for 4 h, are shown in Figs. 4(b)

and 4(c), respectively. The filled squares represent the average NC diameters calculated for the NCs in each layer, while the bars represent the distribution (minimum-maximum) of diameters.

Figure 4(a) reveals that the average diameter of NCs is nearly independent of annealing time after 1 h. In a two-dimensional layer a spherical  $\text{NiSi}_2$  particle is expected to grow according to a power law of the form  $r \sim t^n$ , where  $r$  is radius of the sphere,  $t$  is annealing time, and  $n$  has a typical value of 1/3.<sup>18</sup> Since nucleation of  $\text{NiSi}_2$  precipitates is expected to proceed rapidly at 1100 °C the constant NC size in the present case suggests that further growth is limited by the supply of Ni or Si.

Figure 4(b) shows that the average NC diameter increases with increasing Ni concentration after annealing for 4 h. This annealing time, as seen in Fig. 4(a), is sufficient for complete growth of the NCs. The size is also affected by the supply of Si, as shown in Fig. 4(c). In this case the diameter also increases with increasing Si concentration. These results suggest that the size of  $\text{NiSi}_2$  NCs can be influenced by varying either the Si or Ni concentration in the  $\text{SiO}_x$  layer.

In summary, it has been shown that  $\text{NiSi}_2$  NCs can be formed in silicon-rich oxide layers containing ion-implanted Ni, and that the size of these NCs can be influenced by limiting either the Ni or excess Si concentration. The resulting NCs are approximately spherical in shape and can be produced with diameters in the range from 5 to 40 nm.

This work was carried out under Scientists Exchange Program between the Korea Science and Engineering Foundation and the Australian Academy of Science, and supported by the Research Grant from the Kangwon National University.

- <sup>1</sup>T. A. Fulton and G. D. Dolan, Phys. Rev. Lett. **59**, 109 (1987).
- <sup>2</sup>L. Zhuang, L. Guo, and S. Y. Chou, Appl. Phys. Lett. **72**, 1205 (1998).
- <sup>3</sup>D. L. Klein, R. Roth, A. K. L. Lim, A. P. Alivisatos, and P. L. McEuen, Nature (London) **389**, 699 (1997).
- <sup>4</sup>S. J. Tans, A. R. M. Verschueren, and C. Dekker, Nature (London) **393**, 49 (1998).
- <sup>5</sup>H. Park, J. Park, A. K. L. Lim, E. H. Anderson, A. P. Alivisatos, and P. L. McEuen, Nature (London) **407**, 57 (2000).
- <sup>6</sup>M. H. Devoret, D. Esteve, and C. Urbina, Nature (London) **360**, 547 (1992).
- <sup>7</sup>D. V. Averin and K. K. Likharev, J. Low Temp. Phys. **62**, 345 (1986).
- <sup>8</sup>M. G. Spooner, T. M. Walsh, and R. G. Elliman, Mater. Res. Soc. Symp. Proc. **770**, 11.8.1 (2003).
- <sup>9</sup>T. Inokuma, Y. Wakayama, T. Muramoto, R. Aoki, Y. Kurata, and S. Hasegawa, J. Appl. Phys. **83**, 2228 (1998).
- <sup>10</sup>D. Nesheva, C. Raptis, and A. Perakis, J. Appl. Phys. **92**, 4678 (2002).
- <sup>11</sup>C. Hayzlden, J. L. Batstone, and R. C. Cammarata, Appl. Phys. Lett. **60**, 225 (1992).
- <sup>12</sup>H. Yang, R. F. Pinizzotto, L. Luo, and F. Namavar, Appl. Phys. Lett. **62**, 2694 (1993).
- <sup>13</sup>X. W. Zhang, S. P. Wong, and W. Y. Cheung, J. Appl. Phys. **92**, 3778 (2002).
- <sup>14</sup>W. W. Wu, J. H. He, S. L. Cheng, S. W. Lee, and L. J. Chen, Appl. Phys. Lett. **83**, 1836 (2003).
- <sup>15</sup>C. A. Decker, R. Solanki, J. L. Freeouf, and J. R. Carruthers, Appl. Phys. Lett. **84**, 1389 (2004).
- <sup>16</sup>Smithells Metals Reference Book, edited by E. A. Brandes and G. B. Brook (Butterworth-Heinemann, Oxford, 1992).
- <sup>17</sup>K. N. Tu, Appl. Phys. Lett. **27**, 221 (1975).
- <sup>18</sup>R. C. Cammarata, C. V. Thompson, C. Hayzelden, and K. N. Tu, J. Mater. Res. **5**, 2133 (1990).